Ab initio study of reflectance anisotropy spectra of a submonolayer oxidized Si(100) surface

André Incze
Istituto Nazionale per la Fisica della Materia and Dipartimento di Fisica dell'Università di Milano, via Celoria 16, I-20133 Milano, Italy
Istituto Nazionale per la Fisica della Materia and Dipartimento di Fisica dell'Università di Roma "Tor Vergata," Via della Ricerca Scientifica, I-00133 Roma, Italy

Rodolfo Del Sole
Istituto Nazionale per la Fisica della Materia and Dipartimento di Fisica dell'Università di Roma "Tor Vergata," Via della Ricerca Scientifica, I-00133 Roma, Italy

Giovanni Onida
Istituto Nazionale per la Fisica della Materia and Dipartimento di Fisica dell'Università di Milano, via Celoria 16, I-20133 Milano, Italy
(Received 23 June 2004; revised manuscript received 11 October 2004; published 31 January 2005)

The effects of oxygen adsorption on the reflectance anisotropy spectrum (RAS) of reconstructed Si(100):O surfaces at submonolayer coverage (first stages of oxidation) have been studied by an *ab initio* density-functional theory local-density approximation scheme within a plane-wave, norm-conserving pseudopotential approach. Dangling bonds and the main features of the characteristic RAS of the clean Si(100) surface are mostly preserved after oxidation of 50% of the surface dimers, with some visible changes: a small redshift of the first peak, and the appearance of a distinct spectral structure at about 1.5 eV. The electronic transitions involved in the latter have been analyzed through state-by-state and layer-by-layer decompositions of the RAS. We suggest that the interplay between present theoretical results and reflectance anisotropy spectroscopy experiments could lead to further clarification of structural and kinetic details of the Si(100) oxidation process in the submonolayer range.

DOI: 10.1103/PhysRevB.71.035350 PACS number(s): 78.68.+m, 73.20.−r, 78.40.−q, 71.15.Qe

INTRODUCTION

The developments in the capability to monitor and to control oxidation of the silicon (100) surface at an atomic-scale resolution are a very important issue in semiconductor device technology. In fact, high-quality gate insulators thinner than 2 nm are today required, due to the continuous downscaling of the metal-oxide-semiconductor devices (see, e.g., Ref. 1).

In the last two decades the adsorption of oxygen on silicon surfaces has been extensively studied, from both experimental and theoretical points of view. In particular, the effects induced by oxidation on the optical properties of the silicon surfaces have been thoroughly studied since the mid-1980s.[2,3] It has been known since then that O_2 adsorption is dissociative, and that preferred final adsorption sites for O atoms are Si-Si bond-bridge positions. More recently, it has been shown that in the case of Si(100) the most favorable adsorption sites for O are the dimer bridge and the backbond site of the down atom of the surface dimer.[4,5] The latter site is slightly favored over the former when insertion of a single O atom is considered. When two oxygen atoms originated by the dissociation of an O_2 molecule are present, then the most favorable configuration that can be reached in a barrierless or almost barrierless reaction (i.e., with oxygen present only on surface sites) is that with one oxygen inserted into the down atom backbond, and the other inserted into the dimer bond.[6,7] It is in fact known that, during the first stages of oxidation, O_2 adsorption and O migration to the dimer backbonds proceed as barrierless (or almost barrierless) reactions, as demonstrated by both experimental[8] and theoretical works.[9,10] Configurations with oxygen moving deeper into the second and/or third layer have been theoretically predicted,[11] but require the overcoming of a non-negligible energy barrier and are not considered here. Further Si(100) oxidation has been shown to proceed in a layer-by-layer manner, giving rise to an oscillatory effect in the surface anisotropy, which has been detected by *in situ* reflectance anisotropy spectroscopy measurements.[12,13] The phenomenon of the growth of a SiO_2 layer over the Si(100) surface, and the related problem of the properties of the Si-SiO_2 interface, have received most of the attention, and several calculations of structural and electronic properties of the interface are available.[14,15] However, what happens in the very first stages of oxidation [below 1 monolayer (ML) coverage] is still poorly known: oxidation of the second layer starts soon,[16] and recent experimental works[13,17] do not focus on the formation of the first layer, which is completed in a very short time (less than 1 s) at the experimentally used O_2 partial pressures.[42] Since reflectance anisotropy spectroscopy is a very sensitive technique, which in the case of the clean Si(100) surface is able to detect small structural details,[18,19] and—in contrast with other characterization techniques based on electrons—can be used *in situ* to monitor the process under manufacturing conditions, we suggest, with the present work, a possible application of reflectance anisotropy spectroscopy (RAS) to shed light on the structural and ki-

netic details of the Si(100) oxidation process in the submonolayer range.

Our aim is to study in a detailed and quantitative way the changes in the RAS features induced by very low concentrations of chemisorbed oxygen on the Si(100) surface. To this end, a layer-resolved analysis of the most relevant low-energy spectral features will be presented.

I. THEORY

The RAS is defined as the difference between the normalized reflectivities measured at normal incidence, for two orthogonal polarizations of light. Throughout this paper, the surface is perpendicular to the x axis, and the z direction is perpendicular to the Si-Si dimers of the reconstructed Si(100) surface. The RAS is hence measured, as a function of the photon energy, as $(\Delta R_y/R)-(\Delta R_z/R)$, where R is the (isotropic) Fresnel reflectivity. Describing the surface within a repeated slab geometry, one can express $\Delta R_i/R(i=y,z)$ for normally incident light as[20]

$$\frac{\Delta R_i}{R} = \frac{4\omega}{c}\mathrm{Im}\frac{4\pi\alpha_{ii}^{hs}(\omega)}{\epsilon_b(\omega)-1}, \tag{1}$$

where i is the polarization direction, $\alpha_{ii}^{hs}(\omega)$ are the diagonal terms of the half-slab polarizability tensor, and $\epsilon_b(\omega)$ is the complex bulk dielectric function.

If the slab has a center of inversion or a mirror plane parallel to the surface ($x\rightarrow -x$ symmetry, in our case), the imaginary part of $\alpha_{ii}^{hs}(\omega)$ can be written, in the single-quasiparticle approximation, as

$$\mathrm{Im}[4\pi\alpha_{ii}^{hs}(\omega)] = \frac{4\pi^2e^2}{\omega^2 A}\sum_{\vec{k}}\sum_{v,c}|V^i_{v\vec{k},c\vec{k}}|^2\delta(E_{c\vec{k}}-E_{v\vec{k}}-\hbar\omega), \tag{2}$$

where $V^i_{v\vec{k},c\vec{k}}$ are the matrix elements of the velocity operator between occupied (v) and empty (c) slab eigenstates at the point $\vec{k}$ in the surface Brillouin zone.[21] A is the slab surface area, while $E_{c\vec{k}}$ and $E_{v\vec{k}}$ are conduction and valence energy eigenvalues, taken as representative of quasiparticle energies. Neglecting the pseudopotential nonlocality,[22] the velocity operator can be replaced by the momentum operator divided by the electronic mass, whose matrix elements $P^i_{v\vec{k},c\vec{k}}$ are easy to evaluate in the plane-wave basis. If the slab has two identical surfaces, α_{ii}^{hs} is simply obtained by dividing by 2 the polarizability of the full slab. There are many cases, however, where one needs to single out the contributions coming from an individual half of the slab, or from regions situated at different depths below the surface. This problem has been recently discussed by some of us[23] and by others,[24,25] and can be solved by introducing a real-space cutoff in the definition of the matrix elements.

This method proved itself very useful for separating surface contributions from bulk and subsurface ones in optical spectra, and has already been applied to the case of the clean Si(100) reconstructed surface.[23] In the real-space cutoff scheme, modified matrix elements $\tilde{P}^i_{v\vec{k},c\vec{k}}$ are needed, which incorporate a function $\theta(x)$ switching from 1 inside the selected region to zero outside the selected region. $\tilde{P}^i_{v\vec{k},c\vec{k}}$ are defined as

$$\tilde{P}^i_{v\vec{k},c\vec{k}} = -i\hbar\int d^3\vec{r}\,\Psi^*_{v\vec{k}}(\vec{r})\,\theta(x)\frac{\partial}{\partial r_i}\Psi_{c\vec{k}}(\vec{r}). \tag{3}$$

The imaginary part of the polarizability is hence given by[23]

$$\mathrm{Im}[\alpha_{ii}^{cut}] = \frac{2\pi e^2}{m^2\omega^2 A}\sum_{\vec{k}}\sum_{v,c}[P^i_{v\vec{k},c\vec{k}}]^*\,\tilde{P}^i_{v\vec{k},c\vec{k}}\delta(E_{c\vec{k}}-E_{v\vec{k}}-\hbar\omega), \tag{4}$$

where both $\tilde{P}^i_{v\vec{k},c\vec{k}}$ and $P^i_{v\vec{k},c\vec{k}}$ (the standard momentum matrix element, calculated without the cutoff function) appear. Working in the reciprocal space, the evaluation of $\tilde{P}^i_{v\vec{k},c\vec{k}}$ requires a double sum over the reciprocal lattice vectors $\{\vec{G}\}$, in contrast to the single sum which yields $P^i_{v\vec{k},c\vec{k}}$.[23,43]

II. COMPUTATIONAL DETAILS

Electronic wave functions and eigenvalues are obtained within the local-density approximation (LDA) to density-functional theory[26,27] (DFT) using a plane-waves basis set. The exchange-correlation energy is evaluated according to the Ceperley and Alder results[28] as parametrized by Perdew and Zunger.[29] The ion-electron interaction is represented by norm-conserving pseudopotentials. Special attention was devoted to the generation of a good norm-conserving pseudopotential for oxygen, in order to achieve a high transferability without requiring too many plane waves for convergence. With this aim, we adopted the Hamann scheme,[30] and optimized the core radii in order to find the best compromise between the basis set convergence and transferability. The latter was checked not only against logarithmic derivatives, but also by performing explicit atomic calculations in several excited configurations. More extensive pseudopotential tests have been performed on three small molecules (SiO, H_2SiO, Si_2O) and on the α-quartz crystalline phase of silica, in order to check the convergence of their structural and electronic properties with respect to the basis set (number of plane waves). As a result, the theoretical length of the Si-O bond is found to converge (within 1%) already at a 30 Ry cutoff for all three molecules. The theoretical values of 1.51 Å (SiO) and 1.52 Å (H_2SiO) compare well with the experimental ones [1.51 Å (Ref. 31) and 1.515 Å (Ref. 32), respectively]. Concerning α-quartz, the calculated lattice constant at 30 Ry is 4.87 Å, to be compared with the experimental value of 4.916 Å.[33]

The Si(100) surface was simulated by a repeated slab of 12 silicon layers and four layers of vacuum. The surface unit cell has been chosen as a (2×2) one, for computational convenience, in order to be able to consider both the (2×1) and $p(2\times 2)$ reconstructions within the same cell. First, the clean surface structure has been determined by a full structural optimization (keeping only the central four Si layers as fixed), using the Broyden-Fletcher-Goldfarb-Shanno minimi-

zation algorithm as implemented in the ABINIT code[34] until the residual forces acting on each atom are less than 0.01 eV/Å. The resulting structure was $p(2\times2)$ reconstructed in agreement with previous results,[35] with a dimer buckling of 0.79 Å. The ground state of the $c(4\times2)$ reconstruction, requiring a different surface unit cell, has also been considered for comparison.

From the structural point of view, the difference between $c(4\times2)$ and $p(2\times2)$ is very tiny: in both cases one has rows of buckled Si dimers, and the buckling [in contrast with the (2×1) reconstruction] *alternates* along those rows. The only difference between $c(4\times2)$ and $p(2\times2)$ consists in the buckling alternation *in the direction perpendicular to the rows*.

Considering that, as shown in Ref. 36, the dimer-dimer interaction is much larger along the rows than between adjacent rows, very small energetic and spectral differences between $c(4\times2)$ and $p(2\times2)$ are to be expected. In fact, from the theoretical point of view, the stabilities of the $p(2\times2)$ and $c(4\times2)$ reconstructions are essentially identical.[35] Recently, *ab initio* calculations have shown that it is possible to induce the formation of $p(2\times2)$ domains by electric fields or charge injection.[37]

Experimentally, the coexistence of $p(2\times2)$ and $c(4\times2)$ domains at very low temperature is supported by recent low-temperature noncontact atomic force microscopy data, which show that almost 12% of the ordered Si(100) surface is $p(2\times2)$ reconstructed.[38] Hence, the $p(2\times2)$ cell can be taken as a realistic model of the clean Si(100) surface.

Two O atoms were then adsorbed on each of the two slab surfaces (in order to preserve the inversion symmetry), which corresponds to a 0.5 ML oxidation. Based on previous *ab initio* calculations of oxygen adsorption on the Si(100) surface,[6,7] we have chosen the most stable configuration that can be reached in a barrierless or almost barrierless dissociation of the molecule: one O atom is in bridge position on a surface Si-Si dimer, and the second O atom is also in bridge position on a nearest Si-Si backbond. Many previous theoretical results[4,5,9] have shown that (i) the preferred adsorption site of an isolated O atom is a Si-Si backbond; (ii) the backbond of the "down atom" of the dimer is strongly preferred over the "up atom" backbond (to the point that if adsorption occurs on the backbond of the up atom, this is sufficient to induce locally the reversing of the buckling); (iii) when an O_2 molecule adsorbs, it dissociates leaving[10] one oxygen atom in the Si-Si surface dimer bond, and the remaining atom in the down atom backbond. We consider hence the configuration denoted by (h) in Ref. 7. The same structure is also considered (denoted by "A") in Fig. 1(a) of Ref. 11. This structure has been selected among the several other total energy minima for two oxygen atoms on Si(100), because it can be immediately reached after O_2 dissociation (unlike structures "D" and "E" of Ref. 11) and can efficiently model the effects of "breaking" one of the surface Si-Si dimers.

III. RESULTS

After oxygen adsorption on the dimer and backbond bridge sites (Fig. 1), and a new full structural relaxation, one of the surface Si-Si dimers is broken (see Table I: the dimer length after oxidation becomes 3.06 Å). Concerning the length of the oxidized Si backbond, we obtain 2.53 Å after O adsorption, to be compared with the 2.60 Å reported in Ref. 4. The structural relaxation remains limited to the immediate neighbors of the O atom, since subsurface layers (second and third silicon layers) are not affected appreciably. The buckling of the nonoxidized dimer, which is expected to be stabilized by O adsorption,[5] increases only very slightly, passing from 0.79 to 0.81 Å.

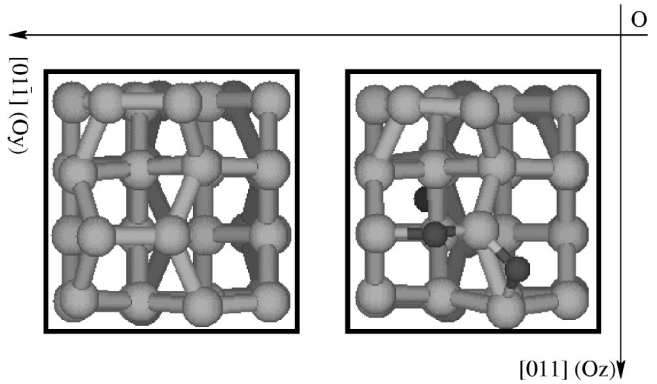

FIG. 1. Top view of the slab after structural optimization, for the clean (left) and oxidized (right) Si(100)-$p(2\times2)$ surfaces. The x axis is perpendicular to the surface, and Si-Si surface dimers are oriented along the y axis.

To compute optical spectra, the ground state calculation must be followed by a calculation of band-structure energies and wave functions over a dense mesh in the irreducible wedge of the Brillouin zone, for both occupied and empty states. With this aim, we calculated Kohn-Sham eigenvectors and eigenvalues using the Arnoldi algorithm,[39] for all states up to 12 eV above the highest occupied state (i.e., about 250 empty states above the 108 filled ones) in each $\vec{k}$ point.

Figure 2 shows the computed band structure, near the Fermi level, for both the clean and the oxidized surfaces, along the ΓKJΓ path in the irreducible wedge of the surface Brillouin zone. For the clean surface, results are in excellent agreement with previous *ab initio* DFT-LDA calculations[35] on the Si(100)-$p(2\times2)$ surface. We note the strong dispersion along ΓK and KJ for the surface bands arising from the dangling bonds which form π (bonding) and π^* (antibond-

TABLE I. Structural changes (Si-Si buckling angle α and dimer length d) at the $p(2\times2)$-reconstructed Si(100) surface, subsequent to 0.5 ML oxidation. Subscript 1 corresponds to the dimer that undergoes oxidation, while subscript 2 to the dimer that remains clean. In parentheses, variations in % with respect to the clean surface. The buckling angles in the case of the clean surface are the averages of two slightly different angles for the two dimers (Ref. 35).

Surface	α_1 (°)	d_1 (Å)	α_2 (°)	d_2 (Å)
Clean	19.2	2.33	19.2	2.33
Oxidized	11	3.06	20.27	2.34
	(−43%)	(+31%)	(+6%)	(0.4%)

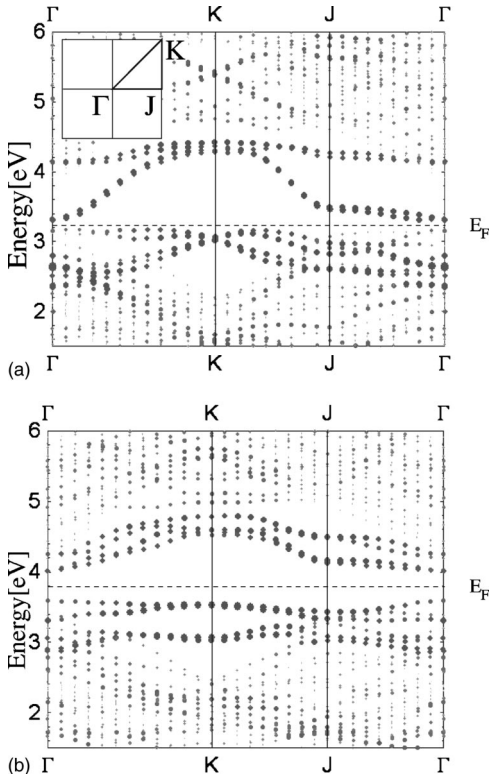

FIG. 2. Surface band structure for Si(100)-$p(2\times2)$, clean (a) and 0.5 ML oxidized (b). Bold dots are used for states that are spatially localized at the surface [integral of $|\Psi_{n\vec{k}}(\vec{r})|^2$ over the two topmost layers larger than 0.5]. The Fermi level has been taken in the middle of the surface band gap.

ing) states. This large dispersion is associated with a non-negligible interaction between adjacent silicon dimers in the direction perpendicular to the dimer axis[36,40] [this is the direction along which the $p(2\times2)$ and $c(4\times2)$ surfaces are identical].

After oxidation, the direct gap at Γ increases from 0.2 to 0.4 eV. However, surface states are still localized on dangling bonds (DBs), as can be seen from a plot (not shown) of their charge densities. Even the oxidized dimers show distinct filled and empty DB-like surface states. The band dispersion in the direction perpendicular to dimers becomes smaller, which can be explained by a weakening of the interaction between adjacent dimers (in our case, an oxidized and a non-oxidized one), as a consequence of oxidation. Oxidation also lifts the initial degeneracy of surface bands at the K corner of the surface Brillouin zone.

Optical spectra have been computed according to Eq. (4), using increasingly large sets of $\vec{k}$ points (up to 162). The following Monkhorst-Pack[41] $\vec{k}$-point meshes were considered in the upper half of the (2×2) surface Brillouin zone: 5×5, 7×7, 9×9, 11×11, and 18×9. In the energy window 0–3.5 eV, the 9×9 mesh is sufficient to achieve convergence, superimposing a small Gaussian broadening (75 meV) to the calculated spectrum. Similarly, in the range between 6 and 12 eV, the 11×11 mesh is sufficient, with the same small broadening. The intermediate energy window, between 3.5 and 6 eV, is the most slowly convergent one.

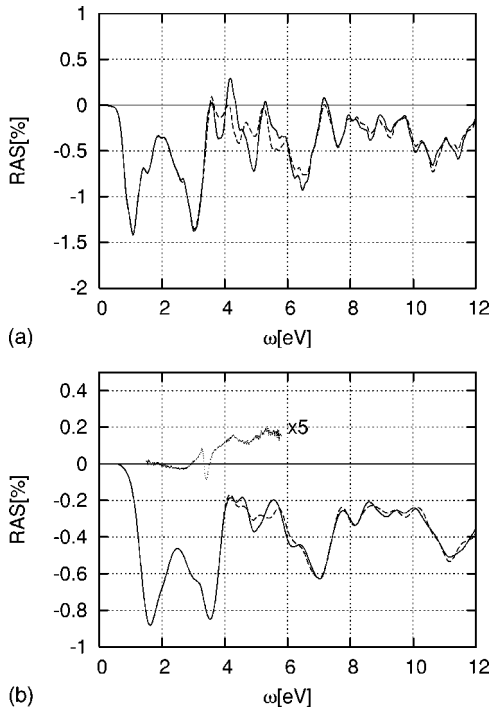

FIG. 3. RAS of the 0.5 ML oxidized Si(100)-$p(2\times2)$, and its convergence with respect to the Brillouin zone sampling. (a): spectra calculated with the 9×9 and 18×9 grids (continuous and dashed lines, respectively), using a Gaussian broadening of 75 meV. (b): spectra calculated with the 11×11 and 18×9 grids (continuous and dashed lines, respectively), using a Gaussian broadening of 250 meV. In the same panel, the lowest-exposure available experimental data from Ref. 12 are reported for comparison: however, the experimental exposure level ($\approx$60 s at 10^{-2} Pa) is nominally much higher than that yielding a submonolayer coverage. Notice that, to facilitate comparison, in this panel the theoretical spectra have been blueshifted by 0.5 eV to correct for the LDA error (scissor operator).

Indeed, a fully converged RAS in this region can only be obtained by increasing the broadening up to 250 meV, with the largest $\vec{k}$-point sets used (11×11 and 18×9). These results are summarized in Fig. 3. In panel (b), the lowest-exposure experimental data from Ref. 12 are also reported for comparison.

Comparing the RAS of the oxidized and clean surfaces up to 1.8 eV two differences come into evidence: (i) after oxygen adsorption, there is a redshift by 0.2 eV of the main transition peak of the clean surface, and (ii) an additional structure appears between 1.4 and 1.75 eV (see Fig. 4). However, the overall RAS line shape does not undergo qualitative changes. In the inset we also plot the RAS of the clean Si(100)-$c(4\times2)$ reconstruction, which below 1.6 eV is practically identical to that of $p(2\times2)$.[44]

In order to clarify the origin and nature of oxygen-induced modifications, we have performed a layer-by-layer analysis of the RAS according to Eqs. (3) and (4), applying the real-space cutoff method described in Ref. 23. This allows one to quantify the contributions to the RAS originating in the different surface and subsurface regions. We divided our slab into five slices: the first four (starting from the

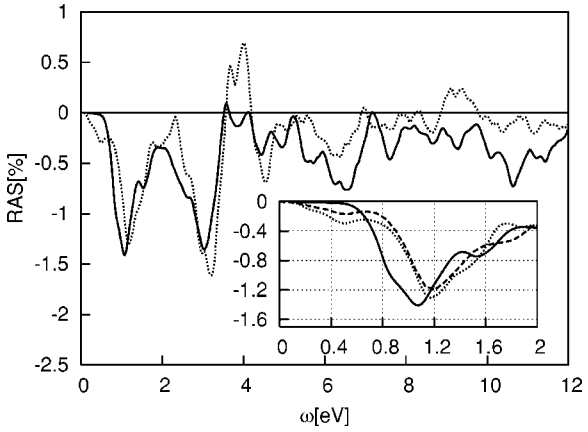

FIG. 4. Effects of the 0.5 ML oxidation on the RAS of Si(100)-$p(2\times2)$: clean surface (dotted line) versus oxidized one (full line). In the inset, the low-energy region is expanded. Besides the oxidized surface (full line) and the clean Si(100)-$p(2\times2)$ (dotted line), we also compare the RAS of the clean Si(100)-$c(4\times2)$ reconstruction (dashed line). A Gaussian broadening of 75 meV has been used.

middle of the slab) containing only silicon atoms, and the last one including surface dimers, oxygen atoms, and the subsurface Si atoms bonded to the surface dimers, as shown in Fig. 5. For the last slice, the cutoff region extends up to a distance of about 1 Å above the surface. The resulting spectra are displayed in Fig. 6: as expected, the reflectance anisotropy signal coming from slices 1 and 2 is almost zero up to 3.0 eV (i.e., in the whole region below the bulk Si direct gap), coherently with the fact that they are bulk representative. The presence of the surface starts to be felt in the third slice, where the two main negative RAS peaks, characteristic of the clean surface, start to appear (at about 1 and 3 eV, respectively). Slice 4 gives a contribution very similar to slice 3, with a larger strength of the 1.0 eV peak. The latter peak is also strongly present in the topmost slice contribution, together with the 3 eV one. An analysis of the localization of electronic states involved in the strongest dipole-allowed transitions for the 1.0 eV peak show almost no contributions from electronic states involving O atoms. Indeed, the states that originate this peak are valence states corresponding mainly to dangling bonds localized on the upper Si atom of the oxidized dimer, and conduction states corresponding mainly to p_x-like orbitals of the lower silicon atom of the nonoxidized dimer. However, besides the two main peaks at 1 and 3 eV, the topmost slice also contributes with an additional structure, located at about 1.5 eV, which does not appear in slice 3 and slice 4 contributions. Empty states involved in the transitions responsible for this feature are in fact found to be strongly localized on the lower Si atom of the Si-O-Si bridge (broken dimer), and on the O atoms themselves (p-like orbitals), so this feature represents a sort of oxygen signature.

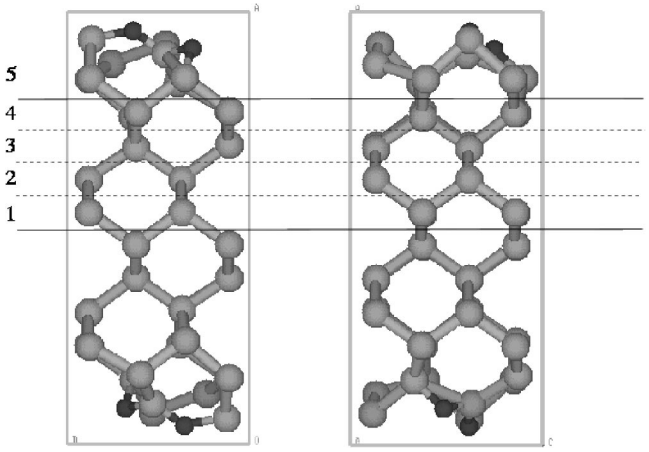

FIG. 5. Side view of the slab, and the slicing used for the layer-by-layer spectral decomposition performed according to the method of Ref. 23. Left: view axis perpendicular to surface dimers. Right: view axis parallel to surface dimers. Darker spheres are used for oxygen, gray ones represent silicon atoms. The oxidized region is fully enclosed in slice 5.

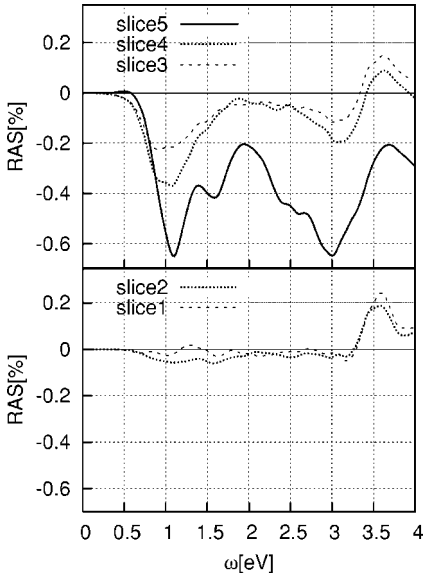

FIG. 6. Results of the layer-by-layer spectral decomposition, according to the slicing displayed in Fig. 5. The spectral feature at about 1.5 eV, recognized as an oxygen signature (see text), comes from the topmost slice only. In contrast, the main peaks at about 1 and 3 eV also include contributions from subsurface states (slices 3 and 4).

In order to obtain deeper insight into the electronic states involved in the main spectral structures, we have singled out, from the whole summation appearing in Eq. (4), the contributions that give the largest oscillator strength and the largest anisotropy, restricted to well-defined energy windows centered on the main low-energy peaks of the imaginary part of the slab polarizability tensor. To this end, we have selected three energy windows, labeled with A, B, and C (Fig. 7), based on the plot of the imaginary part of the half-slab polarizability for light polarization perpendicular (z) and parallel (y) to the silicon dimers. In each region, the contributions coming from each $\vec{k}$ point and band pair (vc) have been sorted on the basis of two criteria: the value of the squared modulus $|P^z_{v\vec{k},c\vec{k}}|^2$, and the value of the anisotropy calculated as $(|P^z_{v\vec{k},c\vec{k}}|^2-|P^y_{v\vec{k},c\vec{k}}|^2)/(|P^z_{v\vec{k},c\vec{k}}|^2+|P^y_{v\vec{k},c\vec{k}}|^2)$. As a result, only the uppermost four valence states (labeled 105–108) and the

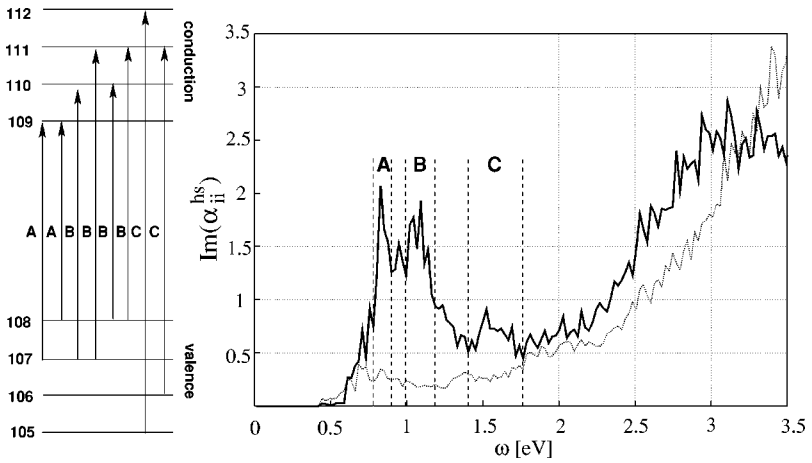

FIG. 7. Contributions of selected slab states involved in the strongest optical transitions for Si(100)-$p(2\times2)$:O, below 1.7 eV. Three energy windows, corresponding to the main spectral features in the imaginary part of the half-slab polarizability tensor $\mathrm{Im}[\alpha_{ii}^{hs}]$, are studied: *A* ([0.8,0.9] eV), *B* ([1.0,1.15] eV), and *C* ([1.40,1.75] eV). The full and dotted lines correspond to light polarization along the *z* and *y* directions, respectively. On the left, we represent schematically the slab states, below and above the Fermi level, and their originated transitions which carry the largest oscillator strength, and anisotropy, in regions *A*, *B*, and *C*.

lowest four conduction states (labeled 109–112) are found to be the main ones responsible for the strongest optical transitions, with $107\rightarrow109$ and $108\rightarrow109$ contributing to peak *A* ([0.8,0.9]eV), and $107+108\rightarrow110+111$ contributing to peak *B* ([1.0,1.15] eV), while peak *C* ([1.40,1.75] eV) is due to the transitions $106\rightarrow111$ and $105\rightarrow112$, as illustrated in Fig. 7.

This result is confirmed by the comparison of the full RAS with a spectrum computed including only this set of four valence and four conduction states (i.e., based on just 16 out of 27 216 *v*-*c* transitions): in the energy window between 0 and 1.8 eV all main features of the RAS are reproduced, apart from small difference in intensities (Fig. 8).

CONCLUSIONS

In conclusion, we have studied the very first stage of oxidation of Si(100)-$p(2\times2)$, at a coverage of 0.5 ML, showing that oxidation of one of the two Si-Si dimers of the $p(2\times2)$ unit cell does not change dramatically the RAS shape, despite the breaking of the dimer and the large flattening of the lowest conduction band, which reflects the weakening of the dimer-dimer interaction along the direction perpendicular to the dimer axis. In particular, the negative peak at 3.7 eV does not disappear (see Ref. 42). However, oxidation of one dimer gives rise to distinguishable effects on the RAS in the lowest-energy region (0 to 1.8 eV), which can be understood in terms of transitions between the four highest valence bands and the four lowest conduction bands of the slab, localized essentially on dangling bonds of silicon atoms, belonging to both types of dimers (oxidized and nonoxidized). These effects are essentially summarized by a redshift of about 0.2 eV of the first RAS negative peak, disappearance of the small structures below 1.0 eV, typical of the clean surface, and appearance of an additional structure at 1.5 eV, which can be seen as an "oxygen signature." The latter can be clearly separated from extra artificial oscillations induced by the discreteness of the Brillouin zone sampling, when a sufficiently large number of $\vec{k}$ points is used. The shift of the first negative peak is strongly linked to the structural surface relaxation which follows oxygen adsorption, and becomes larger if the relaxation is not complete. A layer-by-layer analysis of the RAS shows that the 1.5 eV structure is extremely surface localized (topmost 2.64 Å), while the origin of the two main negative peaks also extends somewhat to the subsurface region (topmost 5.42 Å). We predict that the appearance of this feature should be detectable in reflectance anisotropy spectroscopy experiments on Si(100) in the submonolayer range. Our theoretical predictions could be experimentally assessed by reducing the oxygen exposure to a value of the order of 1–10 L, to be compared with the $\sim10^3$ L of presently available exprimental data.

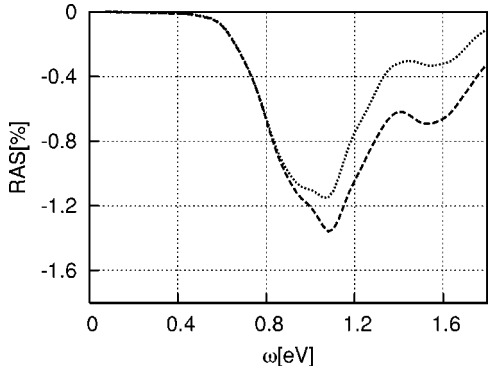

FIG. 8. Contributions of the eight surface states singled out in Fig. 7 to the Si(100)-$p(2\times2)$:O RAS. Dotted line: only 4+4 bands included in the summations of Eq. (4); dashed line: full calculation with 108+250 bands.

ACKNOWLEDGMENTS

We acknowledge the European Community for financial support under the NANOQUANTA project (Contract No. NMP4-CT-2004-500198), and the Italian "Ministero dell'Istruzione, dell Università e della Ricerca" for financial support within COFIN. A. I. also acknowledges support through the EEC under Contract No. HPRNT-CT-2000-00167 (Università Tor Vergata, Roma). We would like to thank C. Hogan, M. Palummo, and M. Gatti for useful discussions, and N. Manini for a careful reading of the manuscript. Computer facilities at CINECA granted by INFM (Project No. 239488704824) are gratefully acknowledged.

[1] I. J. R. Baumvol, Surf. Sci. Rep. **36**, 1 (1999).
[2] A. Selloni, P. Marsella, and R. Del Sole, Phys. Rev. B **33**, 8885 (1986).
[3] E. G. Keim, L. Wolterbeek, and A. van Silfhout, Surf. Sci. **180**, 565 (1987).
[4] T. Uchiyama and M. Tsukada, Surf. Sci. **357**, 509 (1996).
[5] T. Uchiyama and M. Tsukada, Phys. Rev. B **53**, 7917 (1996).
[6] T. Uchiyama, T. Uda, and K. Terakura, Surf. Sci. **433**, 896 (1999).
[7] Y. Widjaja and C. B. Musgrave, J. Chem. Phys. **116**, 5774 (2002).
[8] H. Watanabe, K. Kato, T. Uda, K. Fujita, M. Ichikawa, T. Kawamura, and K. Terakura, Phys. Rev. Lett. **80**, 345 (1998).
[9] K. Kato, T. Uda, and K. Terakura, Phys. Rev. Lett. **80**, 2000 (1998).
[10] K. Kato and T. Uda, Phys. Rev. B **62**, 15 978 (2000).
[11] H. Kageshima and K. Shiraishi, Phys. Rev. Lett. **81**, 5936 (1998).
[12] T. Yasuda, S. Yamasaki, M. Nishizawa, N. Miyata, A. Shklyaev, M. Ichikawa, T. Matsudo, and T. Ohta, Phys. Rev. Lett. **87**, 037403 (2001).
[13] T. Matsudo, T. Ohta, T. Yasuda, M. Nishizawa, N. Miyata, S. Yamasaki, A. A. Shklyaev, and M. Ichikawa, J. Appl. Phys. **91**, 3637 (2002).
[14] A. Pasquarello, M. S. Hybertsen, and R. Car, Nature (London) **396**, 58 (1998).
[15] T. Nakayama and M. Murayama, Appl. Phys. Lett. **77**, 4286 (2000).
[16] K. Nakajima, Y. Okazaki, and K. Kimura, Phys. Rev. B **63**, 113314 (2001).
[17] T. Yasuda, N. Kumagai, M. Nishizawa, S. Yamasaki, H. Oheda, and K. Yamabe, Phys. Rev. B **67**, 195338 (2003).
[18] R. Shioda and J. van der Weide, Phys. Rev. B **57**, R6823 (1998).
[19] U. Rossow, L. Mantese, and D. E. Aspnes, J. Vac. Sci. Technol. B **14**, 3070 (1996).
[20] F. Manghi, R. Del Sole, A. Selloni, and E. Molinari, Phys. Rev. B **41**, 9935 (1990).
[21] R. Del Sole, in *Photonic Probes of Surfaces*, edited by P. Halevi, (Elsevier, Amsterdam 1995), p. 131.
[22] See, e.g., A. Marini, G. Onida, and R. Del Sole, Phys. Rev. B **64**, 195125 (2001).
[23] C. Hogan, R. Del Sole, and G. Onida, Phys. Rev. B **68**, 035405 (2003).
[24] C. Castillo, B. S. Mendoza, W. G. Schmidt, P. H. Hahn, and F. Bechstedt, Phys. Rev. B **68**, 041310(R) (2003).
[25] P. Monachesi, M. Palummo, R. Del Sole, A. Grechnev, and O. Eriksson, Phys. Rev. B **68**, 035426 (2003).
[26] P. Hohenberg and W. Kohn, Phys. Rev. B **136**, B864 (1964).
[27] W. Kohn and L. J. Sham, Phys. Rev. **140**, A1133 (1965).
[28] D. M. Ceperley and B. J. Alder, Phys. Rev. Lett. **45**, 566 (1980).
[29] J. P. Perdew and A. Zunger, Phys. Rev. B **23**, 5048 (1981).
[30] G. B. Bachelet, D. R. Hamann, and M. Schlüter, Phys. Rev. B **26**, 4199 (1982).
[31] G. Herzberg, *Molecular Spectra and Molecular Structure*, 2nd ed. (Van Nostrand Reinhold, New York, 1950).
[32] M. Bogey, B. Delcroix, A. Walters, and J.-C. Guillemin, J. Mol. Spectrosc. **175**, 421 (1996).
[33] L. Levien, C. T. Prewitt, and D. J. Weidner, Am. Mineral. **65**, 920 (1980).
[34] X. Gonze, J.-M. Beuken, R. Caracas, F. Detraux, M. Fuchs, G.-M. Rignanese, L. Sindic, M. Verstraete, G. Zerah, F. Jollet, M. Torrent, A. Roy, M. Mikami, Ph. Ghosez, J.-Y. Raty, and D. C. Allan, Comput. Mater. Sci. **25**, 478 (2002).
[35] A. Ramstad, G. Brocks, and P. J. Kelly, Phys. Rev. B **51**, 14 504 (1995).
[36] M. Palummo, G. Onida, R. Del Sole, and B. S. Mendoza, Phys. Rev. B **60**, 2522 (1999).
[37] K. Seino, W. G. Schmidt, and F. Bechstedt, Phys. Rev. Lett. **93**, 036101 (2004).
[38] T. Uozumi, Y. Tomiyoshi, N. Suehira, Y. Sugawara, and S. Morita, Appl. Surf. Sci. **188**, 279 (2002).
[39] R. B. Lehoucq, D. C. Sorensen, and C. Yang, *ARPACK Users' Guide: Solution of Large-Scale Eigenvalue Problems with Implicitly Restarted Arnoldi Methods* (SIAM, Philadelphia, 1998); www.caam.rice.edu/software/ARPACK
[40] C. Kress, A. Shkrebtii, and R. Del Sole, Surf. Sci. **377**, 398 (1997).
[41] J. D. Pack and H. J. Monkhorst, Phys. Rev. B **16**, 1748 (1977).
[42] The experimental conditions, with an O_2 partial pressure as large as 10^{-2} Pa, lead an exposure at about 10^3 L in only a few seconds. As a consequence, the well-known surface-originating negative RAS peaks at low energy disappear almost immediately (see Figs. 5 and 6 in Ref. 13).
[43] Because of the double sum, the computation of the matrix elements using the cutoff technique can become time consuming, especially when a high cutoff energy is required for convergence. We have checked convergence of the matrix elements calculation over the number of $\vec{G}$ vectors included in the sum. We have obtained that 4000 $\vec{G}$ vectors are enough for achieving convergence, approximatively 1/5 of the initial basis size.
[44] The slight differences between the present results and those of Ref. 36 are due to a present better convergence in the $\vec{k}$-point sampling.